



RESEARCH ARTICLE

Forming submicron in micron texture on the diamond-wire-sawn mc-Si wafer by introducing artificial defects

Chengkun Wu¹  | Shuai Zou^{1,2}  | Jingyan Zhu¹ | Xiaoya Ye² | Jianming Ding¹ | Hua Sun¹ | Xusheng Wang² | Guoqiang Xing² | Xiaohong Zhang¹ | Xiaodong Su¹

¹School of Physical Science and Technology, and Jiangsu Key Laboratory of Thin Films, Soochow University, 1 Shizi Street, Suzhou, 215006, China

²Research & Development Department, Canadian Solar Inc, 199 Lushan Road, SND, Suzhou, 215129, China

Correspondence

Hua Sun and Xiaodong Su, School of Physical Science and Technology, and Jiangsu Key Laboratory of Thin Films, Soochow University, 1 Shizi Street, Suzhou 215006, China.
Email: hsun@suda.edu.cn; xdsu@suda.edu.cn

Funding information

Priority Academic Program Development of Jiangsu Higher Education Institutions; Postgraduate Research & Practice Innovation Program of Jiangsu Province, Grant/Award Number: KYCX19_1967; National Natural Science Foundation of China, Grant/Award Number: 91833303; Key University Science Research Project of Jiangsu Province, Grant/Award Number: 16KJA140002

Abstract

Based on a traditional acid etch system (i.e., HNO_3/HF), a complex texture comprising microscale and submicroscale structures was produced on the surface of a diamond-wire-sawn (DWS) multicrystalline Si (mc-Si) wafer, upon whose surface it is typically difficult to form an effective texture for suppressing the reflection of incident light. Immersing the as-cut wafer into an $\text{HF}/\text{HNO}_3/\text{AgNO}_3$ solution introduced a large number of artificial defects onto the wafer surface. A subsequent HNO_3/HF etch induced a micron texture expanded from the original DWS-induced damage as well as a submicron texture converted from the artificial defects. The multiscale textured DWS exhibited a reflectivity of $\sim 19\%$, which is much lower than the reflectivity after only an HNO_3/HF etch ($\sim 28\%$). Therefore, the solar cell performance was improved owing primarily to improved optical antireflection and surface passivation. The method is simple and can be easily scaled up into the in-line texture process.

KEYWORDS

artificial defects, diamond wire saw, HNO_3/HF etch, in-line texture process, multicrystalline Si solar cell, multiscale texture

1 | INTRODUCTION

Typically, texturing of traditional multiwire slurry-sawn multicrystalline silicon (mc-Si) solar cells is accomplished in an HF/HNO_3 solution via an inline etching machine, producing a relatively high reflection (i.e., $\sim 24\%$) and thus a moderate efficiency below 19% .^{1–4} In the past few years, the cost-effective diamond wire saw (DWS) technique has been adopted overall for slicing mc-Si ingots into wafers. Owing to the reduction of saw-induced damage on the wafer surface from the DWS technique, however, the $\sim 28\%$ reflection of a DWS mc-Si wafer after the traditional HF/HNO_3 texture process results in a low cell power conversion efficiency of $\sim 18.5\%$.^{5, 6} Fortunately, the metal-catalyzed chemical etching (MCCE) technique has

resolved the effective texture problem of DWS mc-Si wafers by introducing a submicron texture onto the surface. This submicron texture exhibits an excellent antireflection ability in a wide spectrum ranging from 300 to 1100 nm, thus promoting the efficiency of mc-Si solar cells to over 19% .^{7–11}

In the present mass production line of Ag-MCCE process, DWS mc-Si wafer are first dipped into a KOH-based solution to remove damage layers, leading to $\sim 2.5\%$ loss of weight. The wafers are then etched in an $\text{HF}/\text{H}_2\text{O}_2/\text{AgNO}_3$ mixed solution to form a nanostructure texture on the wafer surface.^{12, 13} Finally, a postetching process based on an acid etch (HF/HNO_3) has been developed to reduce the strong surface recombination by converting the nanostructures (~ 100 nm) into submicroscale structures (~ 800 nm).¹⁴ Currently, Chinese solar photovoltaic factories have accomplished greater than 20-GW MCCE capacity of DWS mc-Si solar cells. However, the Ag-

Chengkun Wu and Shuai Zou contributed equally.

MCCE process remains unsuitable for some manufacturers owing to the equipment cost, productivity restriction, and the inconvenience of using additional chemicals.

Therefore, two mainstream processes exist for texturing DWS mc-Si wafers in the market, including the traditional acidic process via the inline etching machine and the MCCE process via the bath etching machine. The MCCE process consists of a series of baths whereby the wafers are immersed into either an acidic solution or a hot alkali solution, creating a complicated procedure with a high power and water consumption. In contrast, the acidic inline etching process uses few cassettes working in a floating etch-type process at ambient temperature. This process ensures that the wafer is textured only on the front surface, whereas the back surface can be easily polished to meet the requirement of the passivated emitter and rear cell. This is a significant conservation of chemical, power, and water consumption.¹⁵ With more MCCE batch texturing machines coming to market, more and more inline texturing machines will become obsolete. Therefore, it is critical that the inline acidic process is updated to meet the requirement of efficient mc-Si solar cells.

The etching process proposed in this work is based on the traditional HF/HNO₃ system, where only a trace amount of Ag ions is added into the etching process. Assisted by the HF/HNO₃, the Ag ions introduce a number of artificial defects into the wafer surface. These defects are then etched by the HF/HNO₃ to form a hierarchical submicron and micron texture. Unlike the isolated HF/HNO₃ or Ag-MCCE texture processes, the recipe of the chemical components in the combined etch process can be optimized to form a unique submicron-in-micron (SIM) texture. Further, this process can be scaled to match the acidic inline process and equipment. The DWS mc-Si solar cells with the SIM texture exhibit a significant improvement of the open-circuit voltage (V_{oc}), fill factor (FF), and efficiency (η) over the solar cells treated with the traditional acidic texture process. These values are even slightly higher than the solar cells produced via the Ag-MCCE process owing to the SIM texture with better overall spectral response as well as its relatively low surface and Shockley–Read–Hall recombination loss.

2 | EXPERIMENT

In this work, the DWS mc-Si (100) wafers ($15.6 \times 15.6 \times 0.18$ cm³, p-type, specific resistance $\rho = 1\text{--}3$ Ω ·cm, GCL Company, China) were used. First, 150 pieces of DWS mc-Si wafers from a single batch were divided evenly into Groups A, B, and C, which were, respectively, treated using the traditional HF/HNO₃, the Ag-MCCE, and the HF/HNO₃/AgNO₃ etching processes. The starting chemicals were 28% H₂O₂, 69% HNO₃, 40% HF, 6.94×10^{-5} M AgNO₃, and deionized water (DIW), and they are mixed in volume. For Group A, the 50 DWS mc-Si wafers were etched in an acid solution (HF:HNO₃:DIW = 1:3:1.5) at 10°C for 180 s using an inline etching machine produced for an industrial production line by Canadian Solar Inc. For Group B, the 50 mc-Si wafers were etched by the Ag-MCCE process,

whereby the 50 DWS mc-Si wafers were first immersed into a 2% KOH-based solution for 120 s at 80°C to remove the damage layers. Then, the polished Si wafers were etched in an HF/H₂O₂/DIW/AgNO₃ solution (HF:H₂O₂:DIW:AgNO₃ = 1:0.25:3.53:0.03) for 245 s at 35°C to form nanostructures. The Ag particles were subsequently removed in an NH₄OH/H₂O₂ = 1:1.4 solution for 140 s at room temperature. Finally, the wafers were etched in HF:HNO₃:DIW = 1:4:6 at 10°C for 80 s to form the submicron texture. For Group C, artificial defects were introduced into the 50 mc-Si wafers by immersing the wafers in HF:HNO₃:DIW:AgNO₃ = 1:0.6:2.4:0.03 solution at 35°C for 300 s. The Ag particles were subsequently removed in a 69% HNO₃ solution at ambient temperature for 180 s, after which the wafers were etched in HF:HNO₃:DIW = 1:4:6 at 20°C for 120 s to form the SIM texture. The wafers exhibited a mass reduction ~0.4 g in this process. After texturing, the samples were rinsed in water followed by dipping into a 5% HF solution to remove the surface oxide, whereupon the wafers were etched in 1.5-wt% KOH at ambient temperature to remove the porous Si structures. The samples of Groups B and C were processed using experimental bath etching equipment in our laboratory. Finally, all of the wafers of Groups A–C were assembled into solar cells using a standard process: phosphorus diffusion to form a p–n junction emitter, wet etching to remove edge/back pn junctions and the PSG layer, SiN_x deposition to form an antireflection/passivation layer, and screen printing to fabricate the top/bottom electrodes (Figure 1). The microstructure, reflection, external quantum efficiency (EQE), and electrical characteristics of the cells were measured by scanning electron microscopy (SEM; Hitachi, S4800, Japan), reflectometry (Radiation Technology D8, China), and current–voltage measurements (Sinton Instruments, FCT-450, USA), respectively.

3 | RESULTS AND DISCUSSION

The HF/HNO₃ etching and MCCE process both involve local electrochemical reactions between the silicon and the process chemicals, but the different dynamic processes result in different microstructures. First, consider the Si conduction and valence band edge energies of $E_c = -0.45$ V and $E_v = 0.67$ V, respectively, and the potentials of HNO₃/HNO₂ ($E_{\text{HNO}_3/\text{HNO}_2} = 0.94$ V) and the redox potentials of Ag⁺/Ag ($E_{\text{Ag}^+/\text{Ag}} = 0.8$ V). The Ag nanoparticles can be reduced and grown on the silicon surface by injecting holes from Ag⁺ into the valence band of silicon owing to the much more positive potential of Ag⁺/Ag than the E_v of Si. Meanwhile, HNO₃ can also inject holes into the Ag particles and dissolve them.¹⁶ Typically, it is difficult to reduce Ag on a silicon surface in the presence of HNO₃ owing to the strong dissolution effect, and it is critical to adjust the ratio of chemical components in the system to maintain a balance between the reduction and dissolution of Ag. In proper conditions, the reactant SiO₂ under Ag particles is gradually dissolved by HF to produce H₂SiF₆, thus leaving micropores on the wafer surface.^{17, 18} In this work, these micropores are termed “artificial defects” to distinguish them from the original defects produced during the sawing process.

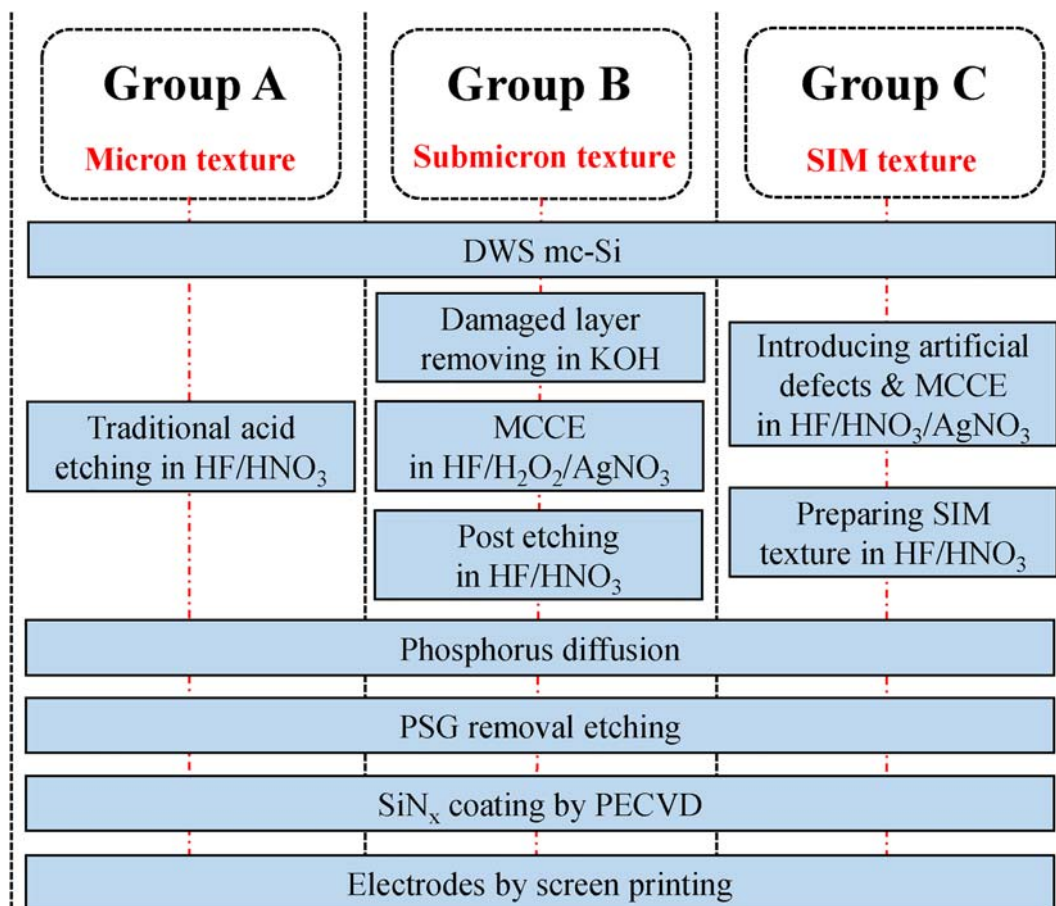


FIGURE 1 Process flow for fabricating DWS mc-Si solar cells with various textures [Colour figure can be viewed at wileyonlinelibrary.com]

Figure 2 is an illustration of the four main steps for the fabrication of the SIM texture on the DWS mc-Si wafers. Though many parallel saw marks exist on the surface of the as-cut wafer, these are inadequate as a starting point for traditional HF/HNO₃ etching to form an effective texture.¹⁹ When etching in the HF/HNO₃/AgNO₃ mixture solution, the Ag-loaded region of the silicon wafer can be dissolved and orderly nanostructures are ultimately formed on wafer surface.²⁰ After removing the remaining Ag particles,

these nanostructures can act as artificial defects introduced onto the wafer surface, thus altering the etch behavior in HF/HNO₃ solution. In this way, the usual micron texture will be produced by expanding the saw damage, and simultaneously, a submicron texture will be formed from the artificial defects. Therefore, a unique SIM texture can be ultimately created on the surface of mc-Si that is expected to have a superior antireflection effect compared to the micron texture alone.²¹

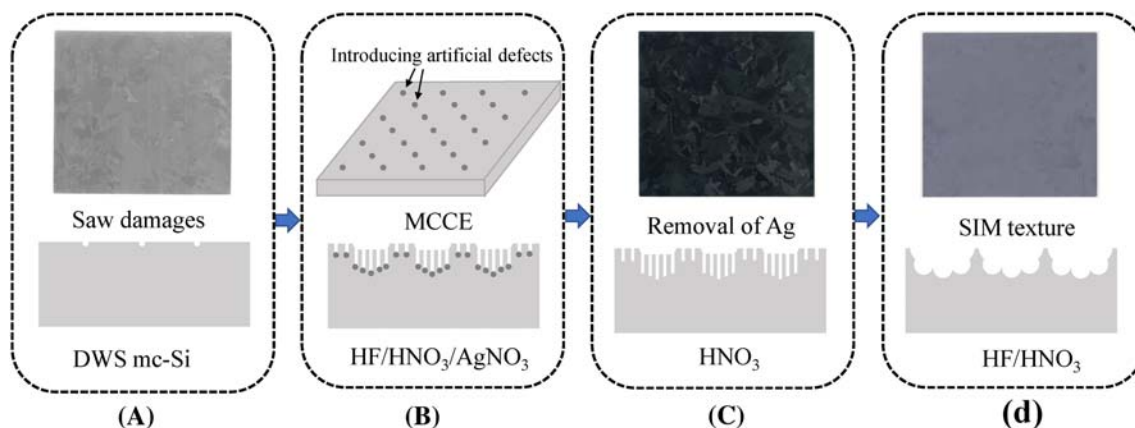


FIGURE 2 Schematic illustration of the main steps to prepare the SIM texture on the DWS mc-Si wafer. (Insets) Wafer photographs in (A), (C), and (D) and schematic in (B) [Colour figure can be viewed at wileyonlinelibrary.com]

Figure 3 compares the SEM images of DWS mc-Si wafers in different etching conditions. For the as-cut wafer (Group A), the saw marks are seen as parallel distributions of fragmentary potholes 3–5 μm in size (Figure 3A). Here, we define the parameter r as the molar ratio of $[\text{HF}]/([\text{HF}] + [\text{HNO}_3])$. After etching in traditional HF/HNO_3 solution with $r = 45\%$, shallow oval-shaped pits several micrometers in size are formed, mostly along a certain direction, leaving the saw marks still visible (Figure 3B).^{2, 15} For the Group B wafers, the saw damage layer of the DWS mc-Si wafer is removed in the KOH -based solution to form a smooth surface (Figure 3C), whereupon a submicron texture about 800 nm in size is formed by the Ag -MCCE process (Figure 3D).^{11, 22} Note that the intensity differences among the differently oriented grains are increased after the anisotropic alkali polishing of the Ag -MCCE process.

To introduce artificial defects on the wafer surface using $\text{HF}/\text{HNO}_3/\text{AgNO}_3$, we performed a systemic experiment to optimize the concentration of AgNO_3 and the ratio of etchant and oxidant. Maintaining the AgNO_3 concentration at $6.94 \times 10^{-5} \text{ M}$, the etching rate of the silicon wafer gradually increased as r was decreased from 90% to 80%, mainly owing to the increased concentration of HNO_3 in the etch solution.¹⁶ In this HF -rich condition, Ag still could be reduced and adhere to the Si surface owing to the comparable reduction potentials of Ag ($E_{\text{Ag}^+/\text{Ag}} = 0.8 \text{ V}$) and HNO_3 ($E_{\text{HNO}_3/\text{HNO}_2} = 0.94 \text{ V}$).¹⁷ However, the Si wafer surface was gradually polished and a negligible amount of Ag particles adhered to the Si surface as r was decreased

from 80% to 40%, implying that the high HNO_3 ratio has a strong Ag dissolution effect. This result explains why the artificial defects cannot be formed in the traditional HNO_3 -rich etching system with $r = 45\%$.

Figure 4 shows SEM images of the morphology evolution of the silicon wafers in Group C during the SIM texture process. After etching in the $\text{HF}/\text{HNO}_3/\text{AgNO}_3$ solution with the optimized $r = 82.7\%$, the nanoscale artificial defects were randomly formed on the wafer surface and the saw marks were almost invisible owing to light scattering effect of the artificial defects (Figure 4A). The cross-sectional SEM image of the artificial defects in Figure 4B demonstrates that they have a diameter $\sim 300 \text{ nm}$ and are not always perpendicular to the surface. Further, the defect depth ranges between 300 and 900 nm (inset of Figure 4B), which is much less than the ~ 1 - to 5 - μm depth of the saw damage layer.² Nevertheless, these artificial defects can be incorporated into the wafer surface with the optimized $r = 82.7\%$ and a trace Ag^+ addition ($<1 \text{ ppm}$). After this process, wafer reflectance was below 3% in the large wavelength region of 300–1100 nm (see Figure S1).

After removing the Ag nanoparticles in 69% HNO_3 , the wafer possessed both the saw damage and the artificial defects. Therefore, a complex texture containing microscale and submicroscale structures was ultimately formed on the surface after immersing the wafer into a HF/HNO_3 ($r = 38\%$) solution for 60 s at 10°C (Figure 4C,D). Clearly, a large micron texture ($\sim 2 \mu\text{m}$) was produced, mainly owing to the saw damage defects, whereas the submicron texture ($\sim 600 \text{ nm}$) was

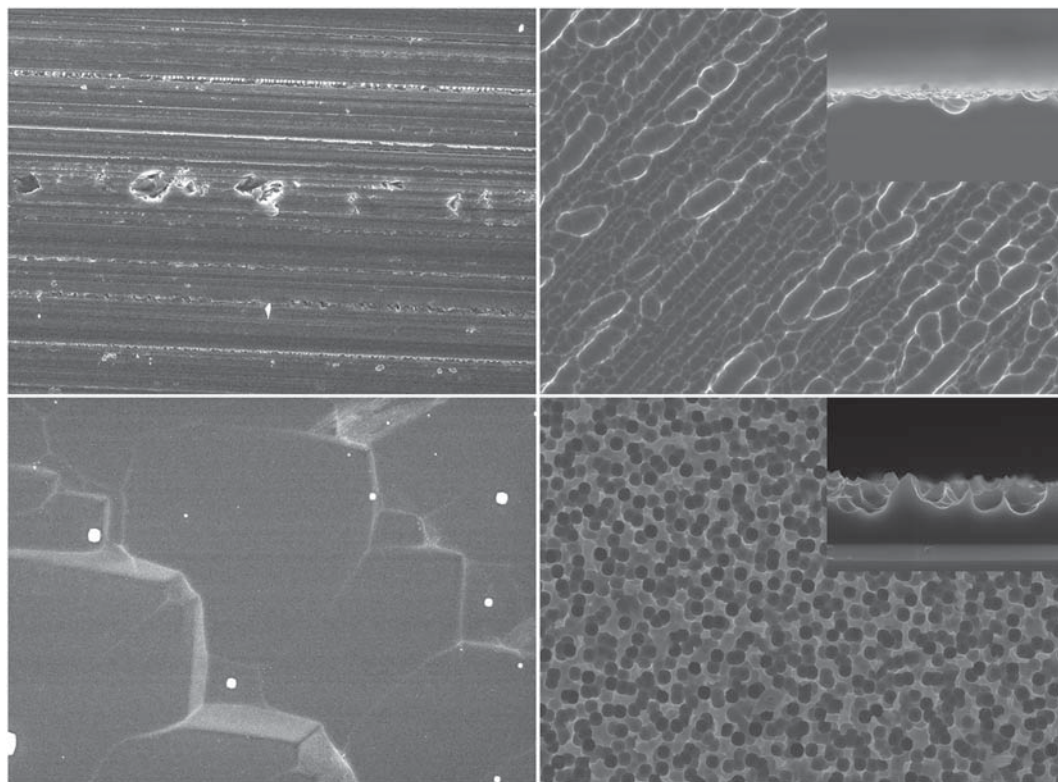


FIGURE 3 SEM surface images of the DWS mc-Si wafers from (A,B) Group A and (C,D) Group B; showing the Group A wafer (A) as-cut, and (B) after etching in HF/HNO_3 (inset: cross-section image), and the Group B wafer after (C) polish-etching in a KOH solution, and (D) after Ag -MCCE process (inset: cross-section image)

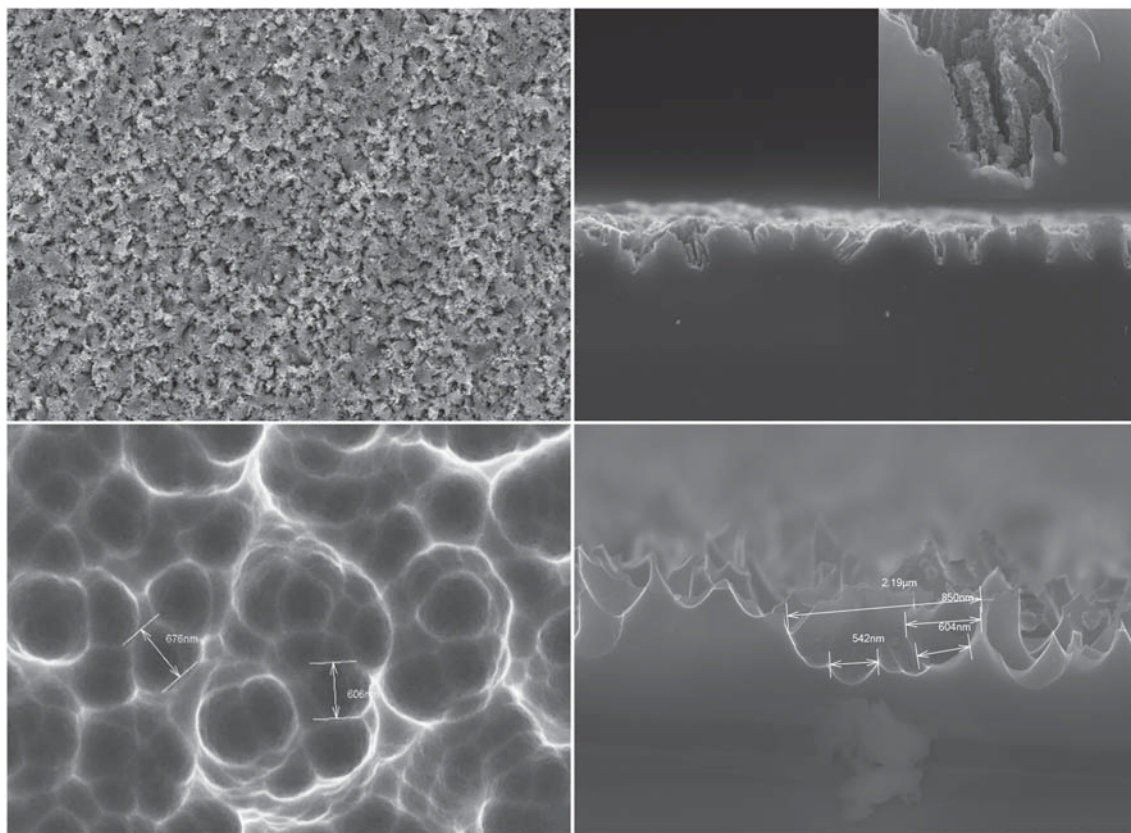


FIGURE 4 SEM surface images of the DWS mc-Si wafer from Group C, (A,B) after etching in HF/HNO₃/AgNO₃ to produce artificial defects, showing (A) surface and (B) cross-section images of the artificial defects; (inset: high magnification of the cross-section morphology of a deep structure). (C,D) After postetching in HF/HNO₃ solution to form SIM texture, showing the (C) surface and (D) cross-sectional image of the SIM texture

converted from the artificial defects. This hierarchical SIM texture is similar to previously reported multiscale surface textures and will similarly exhibit an improved antireflection effect.²¹ In particular, the sub-micron texture is incorporated within the inner spaces of the micron texture and is thus capable of absorbing sunlight via multiple reflections.²³

Figure 5 compares the EQE as a function of wavelength for the entire spectrum of 300–1100 nm among the differently textured DWS mc-Si solar cells. The Group B and Group C samples clearly exhibited a better response in the blue wavelengths than that of Group A owing to the lower reflectance in the 350–700 nm wavelength range (Figure 6), indicating that the submicron texture has a good antireflective performance. Although the Group C samples (i.e., SIM texture) have a higher reflectance than the Group B samples (i.e., Ag-MCCE texture) in Figure 6, the EQE values (>700 nm) of the former are greater than those of the latter. This higher EQE value can be attributed to a more efficient optical absorption and more effective carrier collection.²³ It is well accepted that the micron texture (~2.2 μm) contained in the SIM texture has a relatively good trapping effect for the middle and long wavelengths,²⁴ which was further demonstrated herein using simulation results. Additionally, the submicron texture contained in the SIM texture herein is shallower (~300 nm) than the submicron texture fabricated by the

Ag-MCCE process in the production line (~900 nm), leading to a higher surface passivation quality for the former that will be discussed in the following. Interestingly, the appearance of the SIM-textured solar cell is uniform among the different grains, which may lead to an improved average spectral response among different grains according to a previous report.¹¹

To obtain a deeper insight into the optical properties of the different surface textures in our experiments, we performed a numerical simulation of the solar cell structure illuminated by normal incident light, as illustrated in the left inset of Figure 6. Using this, we calculated the reflection spectra for the Group A–C samples based on the rigorous coupled-wave analysis method.^{25–27} The surface textures of the different samples were characterized by densely-arranged holes with half-ellipsoid shapes (Groups A and B) or with a combination of half-ellipsoid shapes of different sizes (Group C), as shown in the right inset of Figure 6. The set structure parameters of the surface textures were based on the SEM results and are listed in Table 1. Herein, D , H , and R represent the opening diameter, depth, and aspect ratio of the microscale hole, respectively, whereas d , h , and r , respectively, represent these same geometric features for the submicron texture within the surface micron texture in Group C. The dielectric functions of the SiN_x antireflection layer, the silicon substrate, and the Al rear electrode were taken from the literature.²⁸

FIGURE 5 EQE curves of DWS mc-Si wafers with various textures. Inset: Scanning images of three types of mc-Si solar cells and the corresponding SEM images of each group [Colour figure can be viewed at wileyonlinelibrary.com]

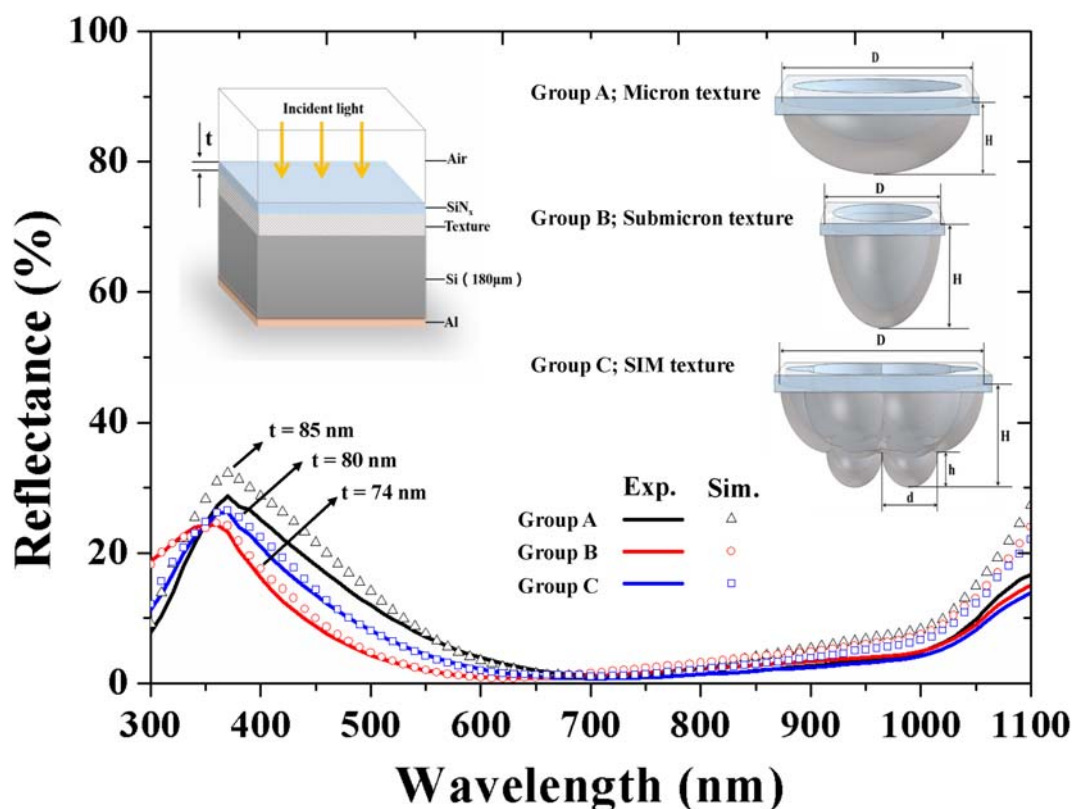
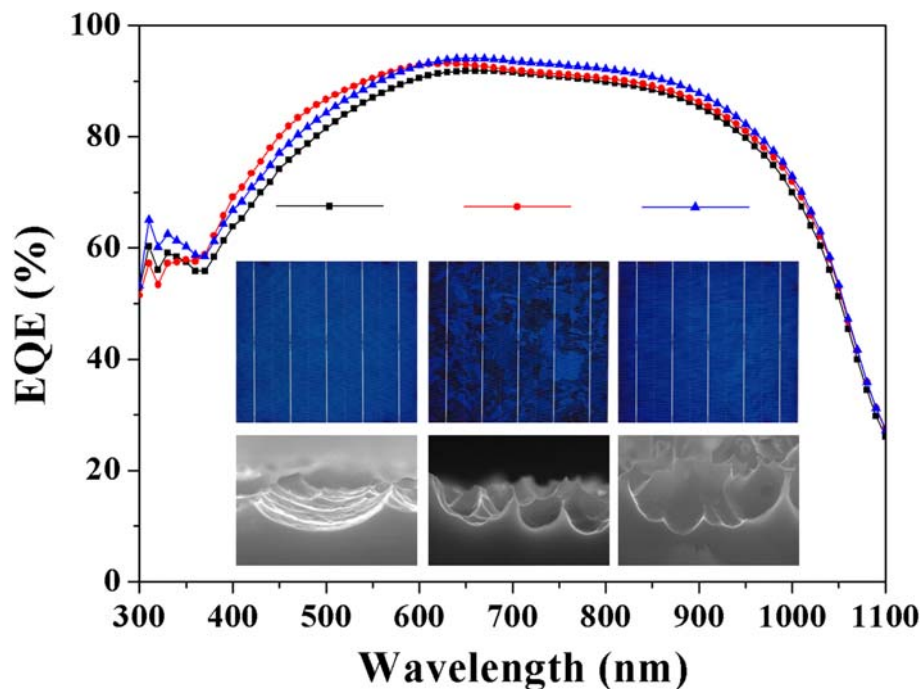


FIGURE 6 Experimental reflectance (curves) and simulated reflectance (scatter points) of three samples. Insets: (left) Schematic diagrams for the simulated cell structure illuminated by normal incident light; (right) structure features of the surface textures, where the values of the structure parameters are listed in Table 1 [Colour figure can be viewed at wileyonlinelibrary.com]

The calculated results of Figure 6 show that the optical properties observed in our experiments are actually the combined effects of both the surface texture and the SiN_x antireflection layer. All of the main

features of the experimentally measured reflection spectra of Groups A, B, and C are successfully reproduced in the simulations when the thickness of the SiN_x antireflection layer was set as 85, 74,

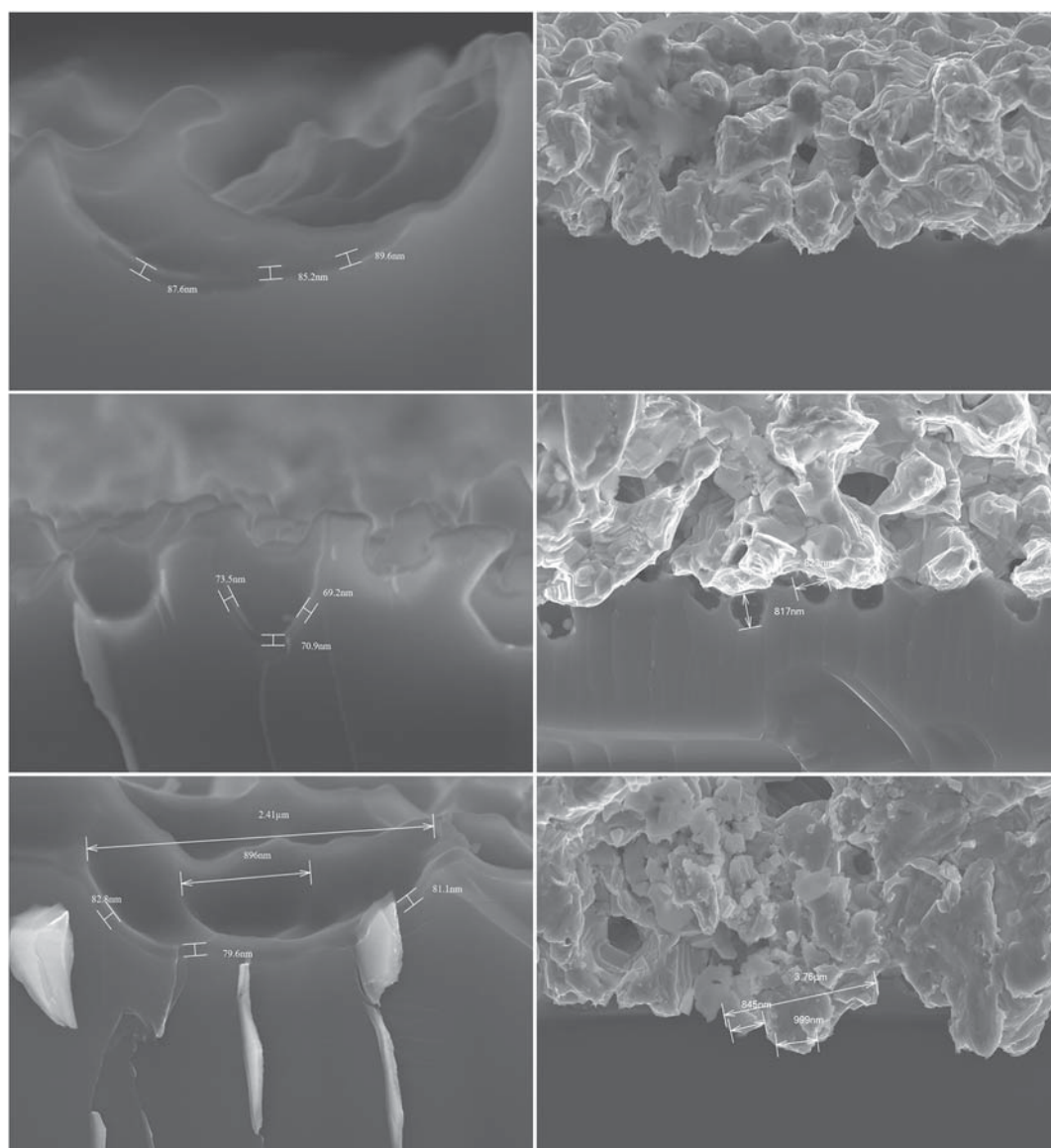
TABLE 1 Structure parameters of the simulated surface textures, including the opening diameter (D , d), depth (H , d), and aspect ratio (R , r) of the micron/submicron texture holes

Sample	D (μm)	H (μm)	d (μm)	h (μm)	$R = H/D$	$r = h/d$
Group A	2.3	0.60	/	/	0.26	/
Group B	0.85	0.84	/	/	0.99	/
Group C	2.2	0.90	0.60	0.30	0.41	0.50

and 80 nm, respectively (Figure 6). In addition, the SiN_x -coated SIM texture in Group C provided the best light-trapping effect for long wavelengths and a comparatively intermediate antireflection for the shorter wavelengths. The difference in the thickness of the SiN_x layer found via the simulations can be attributed to the different surface area increases caused by the surface textures. Specifically, the Group C sample (i.e., SIM texture) tends to form a thicker SiN_x layer than that

of Group B (i.e., submicron texture), which confirms that the former has a smaller surface-area increase and hence a lower surface recombination loss.

Figure 7 presents the cross-sectional SEM images of Si cells in the SiN_x -coated and Ag-Si interface areas. Because all of the samples underwent the same coating process, the differences in the SiN_x thickness are mainly owing to the different textures existing

**FIGURE 7** Cross-sectional SEM images of solar cells showing SiN_x -coated area (left column) and Ag-Si interface area (right column): (A) micron texture in Group A; (B) submicron texture in Group B; (C) SIM texture in Group C

on the Si wafers. The measured thickness of SiN_x of the Group A, B, and C solar cells is ~ 88 , ~ 71 , and ~ 81 nm, respectively (see Figure S2), giving a surface area of Groups B and C that is ~ 1.24 and ~ 1.09 times of that Group A, respectively. In the Group A cell with the micron texture, the SiN_x is in full contact with the Si substrate and maintains the same shape as the micron-textured surface. In the Group B cell with the submicron texture, however, the shape and thickness of the SiN_x is not completely uniform, suggesting that the effect of passivation on the submicron texture is weaker than that on the micron texture. In the Group C cell with the SIM texture, the SiN_x is almost totally conformed to the SIM-textured surface, indicating that the SIM-textured surface can also be effectively passivated by the SiN_x , thus inducing a reduced surface recombination.

From the cross-sectional SEM images of the Ag-Si interface, the textured surface of Group B (Figure 7B) can be seen as not

fully in contact with the SiN_x silver paste. This imperfect contact is mainly owing to the small openings and large depth of the texture that impedes the infusion of silver paste, which results in a poor ohmic contact. In contrast, it is easier for the silver paste to infuse into the micron and SIM textures, (Figure 7A,C, respectively), signifying that these microstructures with the larger openings induces a better ohmic contact (see Figure S3) and thus a smaller serial resistance (R_s). Owing to the relatively good ohmic contact and low surface recombination, the Group C solar cell with the SIM texture exhibits the best performance, and the main cell parameters are shown in Table 2.

To further investigate the electric properties of these three types of solar cells, the values of J_{01} , J_{02} , and pFF were measured by Suns- V_{oc} and are presented in Figure 8. Here, J_{01} describes the recombination of e-h pairs in the base and emitter, and J_{02} illustrates the injection-dependent Shockley-Read-Hall recombination in the space charge region.^{29–31} The pseudo FF (pFF) value disregards the effects of series resistance, thereby avoiding the effect of the Ag-Si series resistance, and the FF value is determined by R_s and pFF . Compared with the solar cells of Groups B and C, the Group A cell has the lowest J_{01} value of ~ 0.58 pA/cm^2 , implying that the micron textures are effectively passivated by SiN_x . Meanwhile, the Group C cell has a slightly lower J_{01} value (~ 0.60 pA/cm^2) compared with the Group B cell (~ 0.61 pA/cm^2), indicating that the SIM-textured surface can be better passivated than the submicron-textured surface. These values

TABLE 2 Main characteristics of mc-Si solar cells with different front textures, including the open-circuit voltage (V_{oc}), short-circuit current (I_{sc}), fill factor (FF), series resistance (R_s), and efficiency (η)

Sample	V_{oc} , mV	I_{sc} , A	FF , %	R_s , $\text{m}\Omega$	η , %
Group A	634.2	8.986	79.58	1.19	18.63
Group B	639.3	9.154	79.84	1.24	19.00
Group C	642.0	9.103	80.18	1.23	19.07

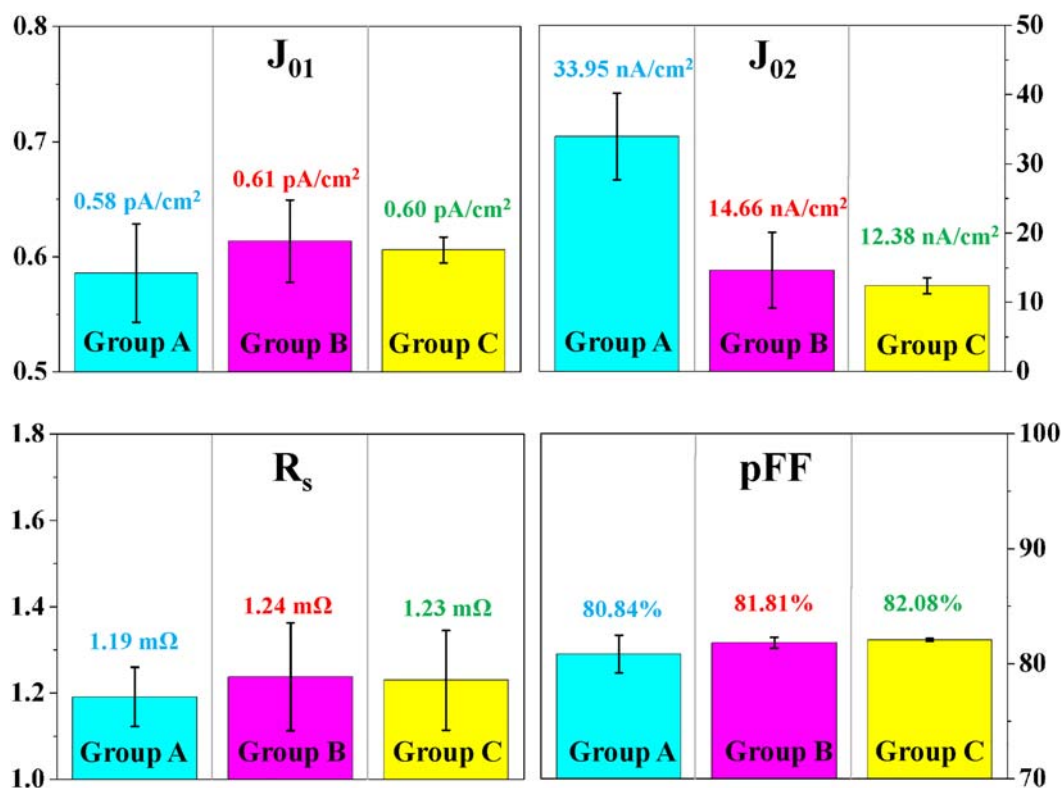


FIGURE 8 Saturation current densities J_{01} (upper left) and J_{02} (upper right) fitted data from the double diode model with ideality $n = 1$ and 2 recombination, respectively; series resistance R_s (lower left) and the pseudo fill factor pFF (lower right) results of DWS mc-Si solar cells with different textures [Colour figure can be viewed at wileyonlinelibrary.com]

are consistent with experimental results shown in Figure 7. The Group A cell has a J_{02} value of ~ 33.95 nA/cm², which is much higher than that of the Groups B (~ 14.66 nA/cm²) and C cells (~ 12.38 nA/cm²), indicating strong Shockley–Read–Hall recombination in the space charge region of the Group A cell. It has been previously demonstrated that this recombination primarily originates from sharp acid etch pits produced by etching in the high-concentration HF/HNO₃ solution (see Figure S4).¹¹

The higher V_{oc} and FF values of the Group B and C cells than those of the Group A cell indicate less recombination loss in the space charge regions of the Group B and C cells, which is in agreement with the lower J_{02} and higher pFF results (Figure 8). We note that a difference of about 3 mV exists between the V_{oc} values of the Group C and B cells, which is possibly owing to the effects of the relatively high surface passivation quality (see Figure S5) and improved p–n junction of the Group C cell that also results in a $\sim 0.34\%$ increase in FF values. Obviously, the lowest short-circuit current value $I_{sc} = \sim 8.986$ A exhibited by the Group A cell is caused by its high surface reflectivity. Furthermore, the decrease of ~ 0.05 A in I_{sc} value exhibited by the Group C cell compared with that of Group B is mainly caused by relatively high loss in the short wavelengths, agreeing well with EQE curves in Figure 5. Ultimately, the average efficiency of the DWS mc-Si solar cells with SIM texture reaches 19.07%, where the texture is created using the in-line texture process of an industrial production line.

4 | CONCLUSION

Based on the refined HF/HNO₃ system and trace AgNO₃, a hierarchical micron and submicron texture structure was produced into a DWS mc-Si solar cell with the help of introduced artificial defects. This unique SIM texture leads an efficiency of $\sim 19.07\%$, which is $\sim 0.44\%$ higher than that of the traditional acid-textured cell. More importantly, unlike the prevalent Ag-MCCE process using the batch-etch process, the SIM texture process is similar to the traditional acid-texture process, enabling the use of the in-line etch process to again produce efficient DWS mc-Si solar cells. Further, both the efficiency and appearance of the SIM-textured solar cells are superior to the Ag-MCCE-textured solar cells owing to the improved passivation, metallization and long-wavelength light trapping.

ACKNOWLEDGEMENTS

This work was supported by the Key University Science Research Project of Jiangsu Province under Grant 16KJA140002, the National Natural Science Foundation of China (Grant 91833303), the Postgraduate Research & Practice Innovation Program of Jiangsu Province (Grant KYCX19_1967), and the Priority Academic Program Development of Jiangsu Higher Education Institutions (PAPD).

ORCID

Chengkun Wu  <https://orcid.org/0000-0002-9566-9932>

Shuai Zou  <https://orcid.org/0000-0003-0630-6687>

REFERENCES

- Zheng CF, Shen HL, Pu T, et al. High-efficient solar cells by the Ag-/Cu-assisted chemical etching process on diamond-wire-sawn multi-crystalline silicon. *IEEE J Photovolt*. 2015;7:153-156.
- Cao F, Chen KX, Zhang JJ, et al. Next-generation multi-crystalline silicon solar cells: diamond-wire sawing, nano-texture and high efficiency. *Sol Energy Mater sol Cells*. 2015;141:132-138.
- Ye XY, Zou S, Chen KX, et al. 18.45%-efficient multi-crystalline silicon solar cell with nano-scale pseudo-pyramid texture. *Adv Funct Mater*. 2014;24(42):6708-6716.
- Chen KX, Liu YY, Wang XS, Zhang LJ, Su XD. Novel texturing process for diamond-wire-sawn single-crystalline silicon solar cell. *Sol Energy Mater sol Cells*. 2015;133:148-155.
- Lin YH, Huang FM, Wu HC, Yeh CH, Chang CC, Chien JW. High efficiency passivated emitter rear contact solar cells with diamond wire saw multi-crystalline silicon wafers. *Energy Procedia*. 2017;130:55-59.
- Wu JT, Liu YP, Chen QS, et al. The orientation and optical properties of inverted-pyramid-like structures on multi-crystalline silicon textured by Cu-assisted chemical etching. *Sol Energy*. 2018;171:675-680.
- Yoo J, Yu G, Yi J. Large-area multicrystalline silicon solar cell fabrication using reactive ion etching (RIE). *Sol Energy Mater sol Cells*. 2011;95(1):2-6.
- Koynov S, Brandt MS, Stutzmann M. Black multi-crystalline silicon solar cells. *Phys Status Solidi RRL*. 2007;1:53-55.
- Koynov S, Brandt MS, Stutzmann M. Black nonreflecting silicon surface for solar cells. *Appl Phys Lett*. 2006;88(20):203107.
- Bastide S, Quang NL, Monna R, Lévy-Clément C. Chemical etching of Si by Ag nanocatalysts in HF-H₂O₂: application to multicrystalline Si solar cell texturization. *Phys Status Solidi c*. 2009;6(7):1536-1540.
- Zou S, Ye XY, Wu CK, et al. Complementary etching behavior of alkali, metal-catalyzed chemical, and post-etching of multicrystalline silicon wafers. *Prog Photovolt Res Appl*. 2019;27(6):511-519.
- Toor F, Oh J, Branz M. Efficient nanostructured 'black' silicon solar cell by copper-catalyzed metal-assisted etching. *Prog Photovolt Res Appl*. 2015;23(10):1375-1380.
- Gondek C, Lippold M, Röver I, Bohmhammel K, Kroke E. Etching silicon with HF-H₂O₂-based mixtures: reactivity studies and surface investigations. *J Phys Chem C*. 2014;118(4):2044-2051.
- Zha JW, Wang T, Pan CF, et al. Constructing submicron textures on mc-Si solar cells via copper-catalyzed chemical etching. *Appl Phys Lett*. 2017;110(9):093901.
- Beaucarne G, Choulat P, Chan BT, Dekkers H, John J, Poortmans J. Etching, texturing and surface decoupling for the next generation of Si solar cells. *Photovoltaics Int*. 2008;1:66-71.
- Kolasinski KW. The mechanism of galvanic/metal-assisted etching of silicon. *Nanoscale Res Lett*. 2014;9(1):432.
- Chen CY, Wong CP. Unveiling the shape-diversified silicon nanowires made by HF/HNO₃ isotropic etching with the assistance of silver. *Nanoscale*. 2015;7(3):1216-1223.
- Steinert M, Acker J, Oswald S, Wetzig K. Study on the mechanism of silicon etching in HNO₃-rich HF/HNO₃ mixtures. *J Phys Chem C*. 2007;111(5):2133-2140.
- Chen KX, Zha JW, Hu FQ, et al. MACE nano-texture process applicable for both single- and multi-crystalline diamond-wire sawn Si solar cells. *Sol Energy Mater sol Cells*. 2019;191:1-8.
- Peng KQ, Hu JJ, Yan YJ, et al. Fabrication of single-crystalline silicon nanowires by scratching a silicon surface with catalytic metal particles. *Adv Funct Mater*. 2006;16(3):387-394.
- Toor F, Branz HM, Page MR, Jones KM, Yuan HC. Multi-scale surface texture to improve blue response of nanoporous black silicon solar cells. *Appl Phys Lett*. 2011;99(10):103501.
- Vázsönyi É, Dúcsó C, Pekker A. Characterization of the anisotropic etching of silicon in two-component alkaline solution. *J Micromech Microeng*. 2007;17(9):1916-1922.

23. Santbergen R, van Zolingen RJC. The absorption factor of crystalline silicon PV cells: a numerical and experimental study. *Sol Energy Mater sol Cells*. 2008;92(4):432-444.
24. Chang CH, Yu P, Hsu MH, et al. Combined micro- and nano-scale surface textures for enhanced near-infrared light harvesting in silicon photovoltaics. *Nanotechnology*. 2011;22(9):095201.
25. Bett AJ, Eisenlohr J, Höhn O, et al. Wave optical simulation of the light trapping properties of black silicon surface textures. *Opt Express*. 2016;24:434-445.
26. Wang P, Azimi S, Breese MBH, Marius P. Near-field enhancement of periodic nanostructures for photovoltaic applications: a theoretical study. *Aust J Optom*. 2014;16(12):125012.
27. Rothmund R, Umundum T, Meinhardt G, Hingerl K, Fromherz T, Jantsch W. Light trapping in pyramidally textured crystalline silicon solar cells using back-side diffractive gratings. *Prog Photovolt Res Appl*. 2013;21:747-753.
28. <https://www.pvlighthouse.com.au/refractive-index-library>.
29. Hussein R, Borchert D, Grabosch G, Fahrner WR. Dark I-V-T measurements and characteristics of (n) a-Si/(p) c-Si heterojunction solar cells. *Sol Energy Mater sol Cells*. 2001;69:123-129.
30. Kunz O, Inns D, Sproul AB, Aberle AG. Application of Suns-Voc and Jsc-Suns measurements to the characterization of Mesa-type thin-film solar cells. Proceedings of the 21st European Photovoltaic Solar Energy Conference and Exhibition, Dresden; 2006: 374-377.
31. Greulich J, Glatthaar M, Krieg A, Emanuel G, Rein SJV. Characteristics of industrial silicon solar cells: influence of distributed series resistance and Shockley Read Hall recombination. Proceedings of the 24th European Photovoltaic Solar Energy Conference and Exhibition. Hamburg; 2009: 2065-2069.

SUPPORTING INFORMATION

Additional supporting information may be found online in the Supporting Information section at the end of this article.

How to cite this article: Wu C, Zou S, Zhu J, et al. Forming submicron in micron texture on the diamond-wire-sawn mc-Si wafer by introducing artificial defects. *Prog Photovolt Res Appl*. 2020;28:788-797. <https://doi.org/10.1002/pip.3271>